View metadata, citation and similar papers at core.ac.uk

brought to you by CORE

provided by DigitalCommons@University of Nebraska

University of Nebraska - Lincoln

DigitalCommons@University of Nebraska - Lincoln

Faculty Publications from Nebraska Center for Materials and Nanoscience

Materials and Nanoscience, Nebraska Center for (NCMN)

6-19-2006

Refractive indices and band-gap properties of rocksalt Mg $_x$Zn sub>1-xO (0.68 ≤x≤1)

Rüdiger Schmidt-Grund
Fakultät für Physik und Geowissenschaften, Institut für Experimentelle Physik II, Universität Leipzig, Linnéstrasse 5, 04103 Leipzig, Germany

Anke Carstens
Fakultät für Physik und Geowissenschaften, Institut für Experimentelle Physik II, Universität Leipzig, Linnéstrasse 5, 04103 Leipzig, Germany

Bernd Rheinländer
Fakultät für Physik und Geowissenschaften, Institut für Experimentelle Physik II, Universität Leipzig, Linnéstrasse 5, 04103 Leipzig, Germany

Daniel Spemann
Fakultät für Physik und Geowissenschaften, Institut für Experimentelle Physik II, Universität Leipzig, Linnéstrasse 5, 04103 Leipzig, Germany

Holger Hochmut
Fakultät für Physik und Geowissenschaften, Institut für Experimentelle Physik II, Universität Leipzig, Linnéstrasse 5, 04103 Leipzig, Germany

See next page for additional authors

Follow this and additional works at: https://digitalcommons.unl.edu/cmrafacpub

Part of the Nanoscience and Nanotechnology Commons

Schmidt-Grund, Rüdiger; Carstens, Anke; Rheinländer, Bernd; Spemann, Daniel; Hochmut, Holger; Zimmermann, Gregor; Lorenz, Michael; Grundmann, Marius; Herzinger, Craig M.; and Schubert, Mathias, "Refractive indices and band-gap properties of rocksalt Mg $_x$Zn sub>1-xO (0.68 ≤x≤1)" (2006). *Faculty Publications from Nebraska Center for Materials and Nanoscience*. 13.
https://digitalcommons.unl.edu/cmrafacpub/13

This Article is brought to you for free and open access by the Materials and Nanoscience, Nebraska Center for (NCMN) at DigitalCommons@University of Nebraska - Lincoln. It has been accepted for inclusion in Faculty Publications from Nebraska Center for Materials and Nanoscience by an authorized administrator of DigitalCommons@University of Nebraska - Lincoln.

Authors

Rüdiger Schmidt-Grund, Anke Carstens, Bernd Rheinländer, Daniel Spemann, Holger Hochmut, Gregor Zimmermann, Michael Lorenz, Marius Grundmann, Craig M. Herzinger, and Mathias Schubert

This article is available at DigitalCommons@University of Nebraska - Lincoln: https://digitalcommons.unl.edu/cmrafacpub/13

Refractive indices and band-gap properties of rocksalt $Mg_xZn_{1-x}O$ ($0.68 \leq x \leq 1$)

Rüdiger Schmidt-Grund,[a] Anke Carstens, Bernd Rheinländer, Daniel Spemann, Holger Hochmut, Gregor Zimmermann, Michael Lorenz, and Marius Grundmann
Fakultät für Physik und Geowissenschaften, Institut für Experimentelle Physik II, Universität Leipzig, Linnéstrasse 5, 04103 Leipzig, Germany

Craig M. Herzinger
J. A. Woollam Co., Inc., 645 M Street, Lincoln, Nebraska 68508

Mathias Schubert[b]
Department of Electrical Engineering and Center for Materials Research and Analysis (CMRA), University of Nebraska-Lincoln, 240N WSEC, Lincoln, Nebraska 68588-0511

(Received 19 April 2005; accepted 25 April 2006; published online 19 June 2006)

The room-temperature optical pseudo-dielectric-functions of single-phase, single-crystalline rocksalt-structure $Mg_xZn_{1-x}O$ with Mg-content x between 0.68 and 1 were determined in the photon energy range from 0.75 to 9.10 eV using spectroscopic ellipsometry. The refractive index determined in the spectral region below the fundamental absorption edge decreases with increasing Mg content. The pseudo-dielectric-functions reveal structures caused in critical points due to electronic band-to-band transitions and free exciton formation at the fundamental band-gap transition. Standard model dielectric function approaches were applied for line shape analysis. Upon increase of the bond ionicity with increasing Mg content the energies of the band-to-band transitions as well as the fundamental-band-gap exciton binding energy parameters increase, while the Γ-point spin-orbit-splitting energy parameter decreases. We compare our results with the band-gap properties of wurtzite-structure $Mg_xZn_{1-x}O$ with Mg-content x between 0 and 0.5 obtained previously, and we discuss discontinuities across the phase transition. We provide estimates for the band gap bowing parameter of rocksalt-structure $Mg_xZn_{1-x}O$ and the band-gap value of rocksalt-structure ZnO. © *2006 American Institute of Physics*. [DOI: 10.1063/1.2205350]

I. INTRODUCTION

Considerable attention is currently devoted to the $Mg_xZn_{1-x}O$ alloy system due to its attractive properties for possible applications in ultraviolet optoelectronics. A large band-gap variation in thin films between the wurtzite-structure ZnO (3.37 eV) (Refs. 1–3) and the rocksalt-structure MgO (7.77 eV) (Ref. 4) is anticipated. Bragg reflector structures consisting of $Mg_xZn_{1-x}O$ layers with high and low Mg contents are of potential interest for ZnO-based optoelectronic devices due to the large variability of the refractive indices. Superlattices structures of MgO and ZnO layers allow tuning of the quasiternary band-gap energy by varying the sublayer thickness values, and may open alternative pathways to the use of ternary materials.[5] Cubic crystalline $Mg_xZn_{1-x}O$ has recently revealed potential for use as high-k dielectric material in silicon technology.[6] The ionicity of the Zn–O bonds compared with the Mg–O bonds are lower. Therefore, for $Mg_xZn_{1-x}O$ with high Mg content one expects high exciton binding energies, which should increase by increasing the Mg content in the crystal. The large value of the exciton binding energy of MgO (80 meV),[4] although comparable to the energy of the optical phonon mode frequency,[7] predicts high-Mg-content material to be advantageous for excitonic light emitters, because the exciton-phonon scattering decreases with an increasing ratio of the exciton binding energy to the optical phonon energy, and which is more favorable than in ZnO. Whereas for small Mg contents the compounds are commonly found to crystallize in the wurtzite-structure, high-Mg-content alloys are of rocksalt structure. While the wurtzite structure composition region is often investigated (e.g., Refs. 1, 2, and 8–15), many optical properties of the rocksalt phase remained unknown so far and further studies are required. Among these properties are the electronic band-to-band transition energies, exciton binding energies, and refractive indices. Successful growth of rocksalt $Mg_xZn_{1-x}O$ films was reported for $x \geq 0.4$.[16–19] Using transmittance measurements, a blueshift of the fundamental band-gap energy E_0 with increasing Mg content x was found, but detail analysis of spin-orbit split ($E_0+\Delta_0$) and of free exciton contributions was not performed. An estimation of the refractive index dispersion was deduced in Ref. 19 from model analysis of thin-film transmittance spectra in the photon energy range between 1.46 and 3.10 eV.

Due to its sensitivity to the complex optical sample response, spectroscopic ellipsometry (SE) provides a valuable tool for determination of dielectric function spectra, even for thin layers.[20] Infrared (IR) dielectric function spectra of rocksalt-structure $Mg_xZn_{1-x}O$ thin films were previously investigated by Bundesmann *et al.*[7] using IR-SE, and static dielectric constant, optical phonon mode frequencies, ampli-

[a]Electronic mail: schmidt-grund@physik.uni-leipzig.de
[b]Electronic mail: mschub@physik.uni-leipzig.de

 © 2006 American Institute of Physics

Downloaded 18 Apr 2007 to 129.93.17.223. Redistribution subject to AIP license or copyright, see http://jap.aip.org/jap/copyright.jsp

tudes, and broadening parameters were derived from dielectric function line shape analysis. In the photon energy range of the electronic band-to-band transitions, which cause typical critical-point (CP) structures in the dielectric function ε, energies, amplitudes, and broadenings of such CP structures can be obtained as best-model parameters from subsequent model dielectric function (MDF) line shape analysis of ε spectra using standard MDF approaches.[20,21] Critical points are connected to Van-Hove singularities within the density of states in the electronic energy-momentum band diagram in zero, one, two, or three dimensions (0D, 1D, 2D, or 3D, respectively) commonly abbreviated by M_0, M_1, M_2, and, M_3-type CP's respectively.[21] With increasing photon energy starting within the band gap of a semiconductor, ε reveals the fundamental absorption edge, which is typically of the 3D-M_0-CP type for direct-gap materials. At higher energies CP structures occur, which are often described as 3D-M_1, or equivalently as 2D-M_0, or M_2-type singularities.[21]

In this paper we focus on the CP structure associated with the electronic polarization near the fundamental band-to-band transition, and report on the model specific parameters for the fundamental-band-gap energies, the fundamental-band-gap exciton binding energies, as well as on the refractive indices of rocksalt $Mg_xZn_{1-x}O$ for Mg contents $0.68 \leqslant x \leqslant 1$. We obtain these information from MDF analysis of SE data taken from thin layers of $Mg_xZn_{1-x}O$ in the spectral range between 0.75 and 9.10 eV.

II. EXPERIMENT

The thin films with thickness values of 100–400 nm and Mg mole fractions of $x=0.68-1$ were grown by pulsed laser deposition (PLD) on *c*-plane (0001) sapphire. The substrate temperature was 750 °C. Rutherford backscattering spectroscopy and x-ray diffraction (XRD) measurements were performed to study the composition and crystal structure of the films, respectively. The XRD results indicate that the single-phase rocksalt structure and the layers are relaxed.[7] SE measurements were performed at room temperature in the photon energy range from 0.75 to 9.10 eV with a spectral spacing of 50 meV and, in addition, within the near-band-gap spectral region in steps of 10 meV.[20] All ellipsometry data were measured at angles of incidence of 60° and 70° using a rotating-analyzer ellipsometer with automated compensator function, where the samples were placed within a dry-nitrogen-purged sample compartment in order to prevent probe light absorption within the vacuum ultraviolet (VUV) spectral region by atmospheric water content. Substantial information on ellipsometry instrumentation and related matter can be found in Ref. 20.[22] All samples were measured as received from the growth process, i.e., without any surface treatment. Storage of samples after removal from the PLD growth chamber was done in dried atmosphere. Native surface over layers and roughness influenced the ellipsometric measurement, in the below-band-gap photon energy region to some extend only, and were accounted for during the numerical model analysis. The surface properties of the samples were investigated using atomic force microscopy (AFM) and render values of the surface roughness in the range between 2 and 25 nm. In Fig. 1, as a typical example for all Mg contents investigated here, the AFM picture of the surface of a $Mg_{0.82}Zn_{0.18}O$ sample is shown. As can be seen, the size of the surface structures is not homogeneous across the sample surface.

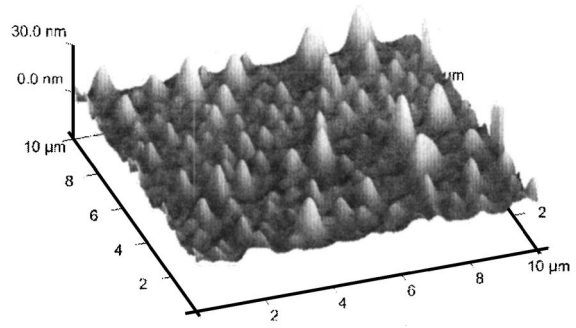

FIG. 1. AFM image of a typical $Mg_xZn_{1-x}O$ surface.

III. THEORY

A. Ellipsometry data analysis

Ellipsometry at oblique angle of incidence Φ determines the ratio ρ of the complex *p*-and *s*-polarized reflectance coefficients r_p and r_s from layered systems with plane parallel interfaces.[20] By definition, in the standard ellipsometry situation Ψ and Δ do not depend on the polarization state of the incident plane wave.[23] Within the Jones presentation the generic expression is

$$\rho = \frac{j_p}{j_s} = \tan \Psi \exp(i\Delta). \tag{1}$$

Here j_p and j_s denote the *p*-and *s*-polarized complex reflection ($j_{p,s}=r_{p,s}$) or transmission coefficients ($j_{p,s}=t_{p,s}$). This situation is applicable to sample systems which behave isotropic, such as for rocksalt-structure single-crystalline thin films on *c*-plane oriented sapphire substrates, i.e., for surfaces which do not reflect (or transmit) *p*-polarized light into *s*-polarized light and vice versa.[24,25] The ellipsometric parameters depend on the photon energy, the sample layer structure, the materials dielectric function, and Φ. The pseudo-dielectric-function $\langle\varepsilon\rangle=\langle\varepsilon_1\rangle+i\langle\varepsilon_2\rangle$, $(i\equiv\sqrt{-1})$, is a common representation of the ellipsometric parameters Ψ and Δ:[26]

$$\langle\varepsilon\rangle = \tan^2\Phi\left[\cos^2\Phi + \sin^2\Phi\left(\frac{1-\rho}{1+\rho}\right)^2\right]. \tag{2}$$

For ellipsometry data analysis, using standard multilayer calculation schemes, a two-layer model is employed here including the *c*-plane (uniaxial) sapphire substrate (the refractive indices were taken from Yao and Yan[27]), the $Mg_xZn_{1-x}O$ layer, and the thin cap layer. Using a Levenberg-Marquardt numerical regression algorithm, the model parameters (layer thickness, MDF parameters) were varied until the model calculated spectra matched the experimental spectra as closely as possible. A weighted test function (maximum likelihood approach) connects measured and calculated data, and related issues of parameter accessibility from spectro-

Downloaded 18 Apr 2007 to 129.93.17.223. Redistribution subject to AIP license or copyright, see http://jap.aip.org/jap/copyright.jsp

TABLE I. Comparison of the surface over layer (SOL) models used in the layer stack model.

	SOL model	Comments
(A)	No SOL	No match between the calculated and experimental data possible.
(B)	BEM.[a] 50% $Mg_xZn_{1-x}O$+50% void	In comparison to (A): one additional parameter.
(C)	BEM: with variable $Mg_xZn_{1-x}O$ to void fraction	In comparison to (A): two additional parameters.
(D)	CA[b]	In comparison to (A): three to four additional parameters.
(E)	BEM: 33% $Mg_xZn_{1-x}O$+33% void+33% CA	In comparison to (A): three to four additional parameters.
(F)	BEM: with variable $Mg_xZn_{1-x}O$ to void to CA material fraction	In comparison to (A): five to six additional parameters.

[a]BEM: Bruggeman effective medium approximation.
[b]CA: Cauchy approximation, cf. Eq. (7).

scopic ellipsometry data have been thoroughly discussed by Jellison in Ref. 20. The experimental error bars on the measured data, which were accounted for appropriately within the test function, were propagated into the error bars on our model parameters. These error bars also represent finite correlation values among the fit parameters. The light propagation within the sample is calculated using standard matrix formalism for multilayered systems with plane parallel interfaces.[20,28]

B. Model dielectric function

For parameterization of the $Mg_xZn_{1-x}O$ dielectric functions ε, two MDF approaches were invoked. The first consists of CP line shape functions (CP-MDF) for determination of the fundamental-band-gap transition energies and exciton binding energies, which is based on the approach suggested by Adachi,[29] including contributions of the 3D-M_0-CP-type (E_0, $E_0+\Delta_0$; Δ_0 is the spin-orbit-split energy) and related free exciton and exciton continuum contributions (exciton binding energy E_{xb}). The contributions of the E_0 and $E_0+\Delta_0$ CP structures to ε are described as follows:

$$\varepsilon^{E_0,E_0+\Delta_0} = A_j E_j^{-1.5}\left[\frac{2-(1+\chi_j)^{0.5}-(1-\chi_j)^{0.5}}{\chi_j^2}\right], \tag{3}$$

with $\chi_j=(E+i\Gamma_j)/E_j$ ($j=0$, Δ_0 for E_0 and $E_0+\Delta_0$, respectively). A_j, E_j, and Γ_j are, respectively, the amplitude, transition energy, and broadening parameter of each CP structure. E is the photon energy. The free exciton contribution at transition energy E_j can be written as

$$\varepsilon^{E_{xb}(E_j)} = \frac{A_{xb}}{(E_j-E_{xb})-E-i\Gamma_{xb}}, \tag{4}$$

where A_{xb} and Γ_{xb} are the discrete exciton strength parameter and the broadening parameter, respectively. Contributions due to band-to-band transitions outside the photon energy range studied were accounted for by a damped harmonic oscillator set to an arbitrary but fixed energy $E_t > E_0+\Delta_0$:

$$\varepsilon^{he} = \frac{A}{E_t^2-E^2-i\Gamma_t E}. \tag{5}$$

The complete CP-MDF in the spectral range investigated here is the sum of the above terms:

$$\varepsilon = \varepsilon^{E_{xb}(E_0)} + \varepsilon^{E_{xb}(E_0+\Delta_0)} + \varepsilon^{E_0} + \varepsilon^{E_0+\Delta_0} + \varepsilon^{he}. \tag{6}$$

In order to provide a more simple parameterization for the below-band-gap index of refraction we further employed a simple Cauchy formula (CA-MDF).[2] The cutoff energy for selecting experimental data for the CA-MDF analysis was set to approximately 90% of the actual band-gap energy E_0. The CA-MDF parameters were assumed to depend on x by second-order polynomials:

$$n(x,\lambda) = A_0 + A_1 x + A_2 x^2 + \frac{B_0 + B_1 x + B_2 x^2}{\lambda^2} + \frac{C_0 + C_1 x + C_2 x^2}{\lambda^4}, \tag{7}$$

where λ is the incident light wavelength in units of microns.

C. Surface over layer effects

The surface of the thin films potentially is not ideal, where roughness and/or surface contaminants may be generally present. For accurate determination of the $Mg_xZn_{1-x}O$ refractive index dispersion and MDF parameters, the effect of the surface must be removed numerically. The results from AFM studies suggest to model the surface roughness effects by inclusion of a surface over layer into the model calculation, where the dielectric function of the surface over layer is estimated by the Bruggeman effective medium approximation weighing the dielectric functions of the $Mg_xZn_{1-x}O$ layer and void ($\varepsilon=1$), which is a common approach.[20] Alternatively, the surface over layer can be modeled due to a transparent layer using a Cauchy approach for the refractive index dispersion [cf. Eq. (7)] or with Bruggeman effective medium approaches consisting of three materials.

In order to highlight the influence of the cap layer on the $Mg_xZn_{1-x}O$ refractive index dispersion and MDF parameters, we have applied different approaches (A)–(F) (Table I) for the model of the surface over layer. For the approaches (B)–(F), comparable good quality of the fit was reached. Consid-

Downloaded 18 Apr 2007 to 129.93.17.223. Redistribution subject to AIP license or copyright, see http://jap.aip.org/jap/copyright.jsp

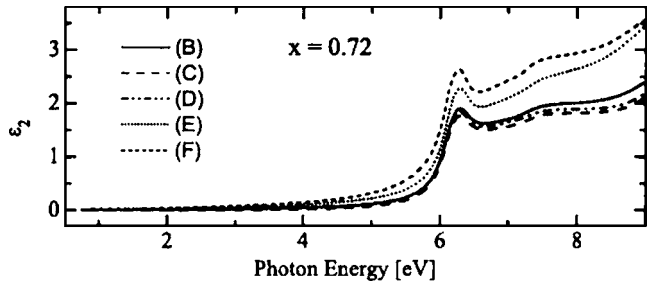

FIG. 2. Spectra of $Mg_xZn_{1-x}O$ dielectric functions ε_2 obtained from the MDF analysis using the surface over layer models (B)–(F) listed in Table I exemplarily for $x=0.72$.

ering the number of parameters used in the fit procedure, model (B) is preferable. Therefore, with lacking accurate data for the actual surface over layer optical constants, we have used the Bruggeman effective medium approximation and set the fraction of the $Mg_xZn_{1-x}O$ and void dielectric functions to be 50% each thereby avoiding the effect of correlation between the surface over layer thickness and the void fraction parameters in this approach. The validity of this treatment is supported by the AFM studies, from which, in consideration of the nonuniformity of the size of the surface structures, average $Mg_xZn_{1-x}O$ and void fractions of 50% each can be estimated (cf. Fig. 1). While the precise determination of the cap layer dielectric function is not of concern here, this approach accounts satisfactorily for the influence of the cap layer on to the measured ellipsometric spectra as long as the overlayer thickness remains small as compared to the wavelength. The cap layers were found from our numerical model analysis with thickness values of 7–14 nm, which match good with the surface roughness values obtained by the AFM investigations.

Likewise, an over or underestimation of the cap layer dielectric function done thereby may affect the absolute value of the $Mg_xZn_{1-x}O$ dielectric function ε, whereas the energies of the CP structures are influenced only little by the absolute values of ε. The uncertainty introduced thereby onto the index of refraction in the transparency region of the $Mg_xZn_{1-x}O$ layers, estimated using the models listed in Table I, is lower than ±0.004 (at 0.75 eV) and ±0.02 (at 90% of the actual band-gap energy E_0) and is within the error bar specified in Sec. IV below. The contributions to the uncertainties of the MDF parameters E_0, Δ_0, and E_{xb} which originated in different surface modeling amount to maximal ±0.007 eV, ±0.02 eV, and ±2 meV, respectively, which is within the error bars given in Fig. 7. The influence of the surface modeling on the $Mg_xZn_{1-x}O$ dielectric function ε is exemplarily shown in Fig. 2 for $x=0.72$. As can be seen, the different approaches result in height shifts between the dielectric functions which were obtained using the different surface over layer models, and to various sharp onset of the absorption at the fundamental absorption edge (≈6 eV). The energetic positions of the CPs are not significantly influenced.

IV. RESULTS AND DISCUSSIONS

Figure 3 depicts experimental and best-fit calculated data exemplarily for the sample with $x=0.82$. The calculated data

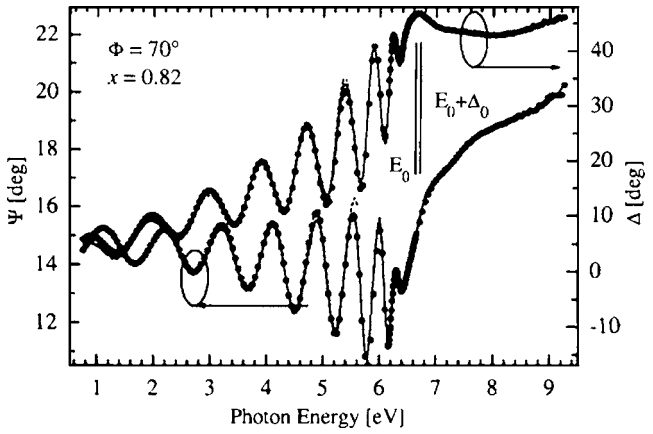

FIG. 3. Experimental (symbols) and best-model calculated ellipsometry data for a $Mg_xZn_{1-x}O$ film deposited on *c*-plane sapphire (CP-MDF: solid lines; CA-MDF: dashed lines). Vertical bars denote transition energies of CP contributions in the near-band-gap spectral region E_0 and $E_0+\Delta_0$.

were obtained by the CP-MDF (entire spectral range) and the CA-MDF (below-band-gap range), as discussed below. The spectra are representative for the samples investigated in this work. Figure 4 summarizes $\langle\varepsilon_2\rangle$ spectra for thin-film samples with representative x values.

A. Below-band-gap index of refraction

For photon energies below E_0 thickness interference effects occur indicating the spectral range of transparency. Figure 5 presents the refractive index dispersions determined upon the CA-MDF analysis [Eq. (7)] within the below-band-gap spectral range. With increasing x, the refractive index n

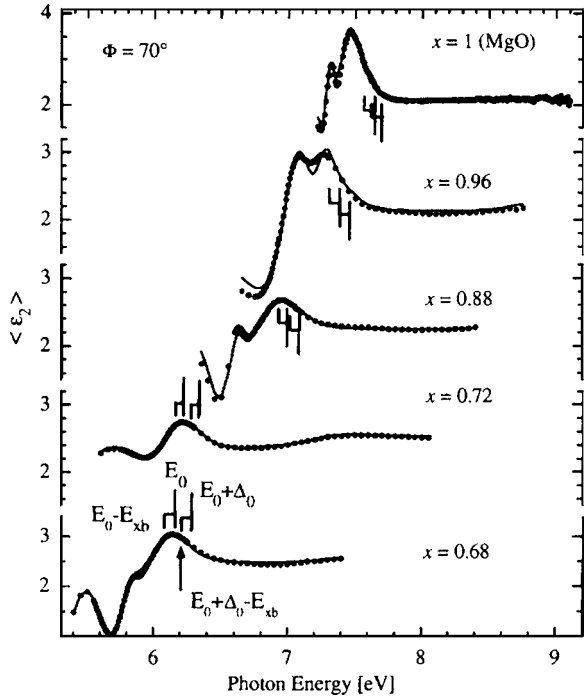

FIG. 4. Experimental (symbols) and best-model calculated (CP-MDF: solid lines) $\langle\varepsilon_2\rangle$ spectra for various $Mg_xZn_{1-x}O$ films deposited on *c*-plane sapphire. Brackets with vertical bars indicate the transition energies E_0 and $E_0+\Delta_0$ (long bar), and their respective exciton resonance E_0-E_{xb} and $E_0+\Delta_0-E_{xb}$ (short bar).

Downloaded 18 Apr 2007 to 129.93.17.223. Redistribution subject to AIP license or copyright, see http://jap.aip.org/jap/copyright.jsp

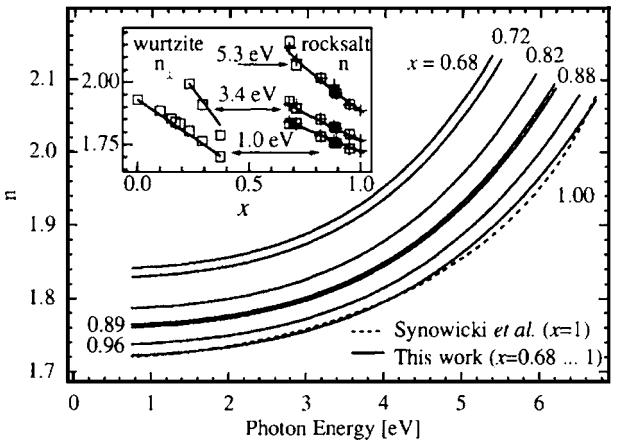

FIG. 5. $Mg_xZn_{1-x}O$ index of refraction n according to Eq. (7) and parameters in Table II (solid lines). For comparison, data reported by Synowicki and Tiwald (Ref. 30) for $x=1$ are included (dashed lines). The inset depicts n for individual photon energies calculated from the best-model CP-MDF (open squares), the best-model CA-MDF for each sample individually (crosses), and for all samples simultaneously (solid lines). Data for the wurtzite part were taken from Ref. 2.

decreases, which resembles previous results for the wurtzite-phase $Mg_xZn_{1-x}O$ system.[2] Data for the refractive index dispersion from SE investigation of a MgO bulk sample in the spectral region from the infrared to vacuum ultraviolet were reported previously by Synowicki and Tiwald.[30] Rocksalt-structure $Mg_xZn_{1-x}O$ thin films with $x=0.57$, 0.70, 0.83, and 1 were studied in the photon energy region 1.46–3.10 eV by Chen *et al.*[19] While the absolute values and the dispersion of n determined in Ref. 30 using SE match our data excellently (cf. Fig. 5), the values of n obtained from model analysis of transmittance spectra using the Manifacier method in Ref. 19 are distinctly lower and overestimate the index dispersion for $x<1$. These differences may originate in uncertainties in the Manifacier-method analysis of the interference pattern of the transmittance intensity spectra.

The inset in Fig. 5 shows the x dependency of the refractive index for $x=0-1$ exemplarily for the photon energies of 1 eV (within the band gap), 3.37 eV (the band-gap energy of ZnO), and 5.3 eV. Note that the wurtzite-structure alloy is optically uniaxial, with small differences between ordinary ($n_\perp$; polarization perpendicular to c axis) and extraordinary ($n_\parallel$, parallel c axis) indices.[2] Similar to the discontinuous composition dependence of E_0 (discussed further below), the refractive index reveals strong discontinuity and increases across the wurtzite-rocksalt-phase transition of the alloy system, which occurs for $x\sim 0.5-0.6$. For example, n for composition $x=0.68$, is similar to $n_\perp$ for $x=0.17$. Extrapolating the $n_\perp$ values for a given photon energy within the wurtzite phase towards compositions within the rocksalt phase would result in much lower indices than observed here. It follows from simple sum rule considerations[31] that the discontinuity in the refractive index must be accompanied by substantial increase in oscillator strengths of higher energy transitions above the spectral range studied here because the discontinuity in E_0, which increases across the phase transition (see below), would otherwise cause a decrease in the refractive index if these oscillator strengths would remain comparable to those within the wurtzite-structure alloy.

TABLE II. Best-model CP-MDF parameters [Eq. (7)] for the x dependency of the below-band-gap index of refraction dispersion of $Mg_xZn_{1-x}O$ ($x=0.68-1$), for photon energies from 0.75 eV to $0.9E_0(x)$.

CA-MDF parameter	Value
A_0	2.146 ± 0.01
A_1	-0.508 ± 0.01
A_2	0.083 ± 0.01
B_0 (μm^2)	$(1.6\pm0.2)\times10^{-2}$
B_1 (μm^2)	$(-2.5\pm0.5)\times10^{-2}$
B_2 (μm^2)	$(1.3\pm0.3)\times10^{-2}$
C_0 (μm^4)	$(1.38\pm0.03)\times10^{-3}$
C_1 (μm^4)	$(-1.48\pm0.05)\times10^{-3}$
C_2 (μm^4)	$(0.36\pm0.04)\times10^{-3}$

The Cauchy parameters according to Eq. (7) are given in Table II. In the inset in Fig. 5, the refractive indices determined using the CP-MDF analysis in the whole spectral range and the CA-MDF analysis in the below-band-gap spectral range done for each sample independently are shown in comparison to n determined by a CA-MDF analysis where all samples were involved simultaneously solving for the x dependency of the CA-MDF parameters given in Table II. The good agreement between the results obtained by the three methods is notable and permits us to conclude that the influence of the surface roughness on the refractive index dispersion is sufficiently well described by the used cap layer model.

B. Near-band-gap dielectric function

Line shape analysis of fine structures in the sample response near the fundamental band-gap energy using the CP-MDF line shape functions [Eqs. (3)–(6)] reveals parameters of the E_0, $E_0+\Delta_0$, and related discrete as well as continuum exciton CP contributions (vertical bars in Figs. 3 and 4). The most prominent structure within the spectra in Fig. 3 originates from the CP structures due to the free exciton and band-to-band transitions at photon energies $\hbar\omega=E_0-E_{xb}$, $E_0+\Delta_0-E_{xb}$, and $\hbar\omega=E_0$, $E_0+\Delta_0$, respectively, followed in the low-energy part of the spectra by thickness interference effects, which are affected by index of refraction dispersion and residual absorption due to band-gap transition broadening. Figure 6 presents the best CP-MDF calculated ε_2 spectra in the near-band-gap spectral region obtained by the CP-MDF analysis with the above described surface over layer model for the $Mg_xZn_{1-x}O$ samples in Fig. 4.[35] The insets show exemplarily the individual CP-MDF contributions due to the excitonic, band-gap, and spin-orbit-split CP's. Note that for reasons of denying any strong correlation amongst the MDF parameters, the broadening parameters were set to be equal for each excitonic respective Γ-point band-to-band transition, the amplitude parameters for the excitonic transitions, and the exciton binding energy for the E_0 and $E_0+\Delta_0$ related excitonic transitions. The exitonic contributions are much stronger than the contribution from the fundamental band-to-band transitions for MgO, but become less pronounced towards higher Zn content. While the individual CP contributions can be clearly differentiated for the MgO

Downloaded 18 Apr 2007 to 129.93.17.223. Redistribution subject to AIP license or copyright, see http://jap.aip.org/jap/copyright.jsp

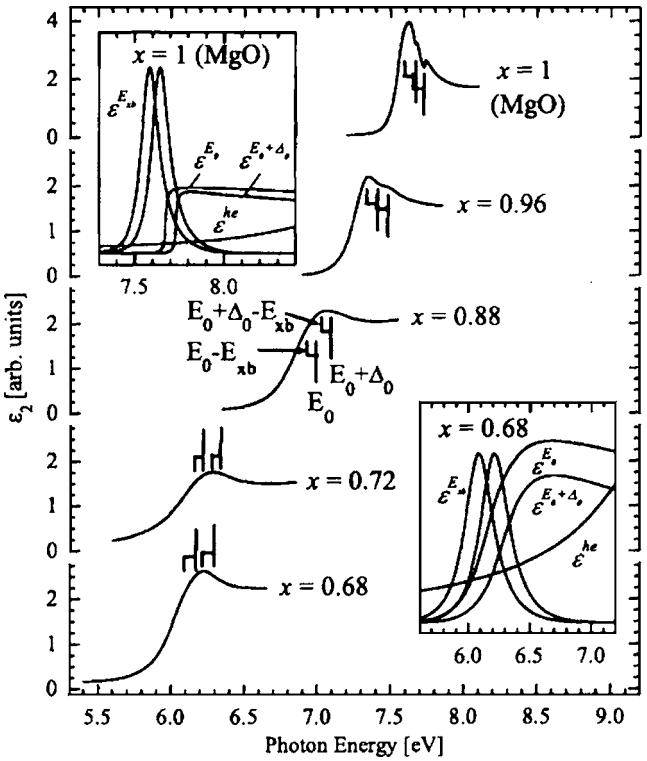

FIG. 6. Calculated ε_2 spectra applying for the used model with the CP-MDF and surface over layer approach described above for the $Mg_xZn_{1-x}O$ samples in Fig. 4. Brackets with vertical bars indicate the transition energies E_0 and $E_0+\Delta_0$ (long bar), and their respective exciton resonances E_0-E_{xb} and $E_0+\Delta_0-E_{xb}$ (short bar), and insets display their individual model contributions exemplarily for $x=1$ and $x=0.68$.

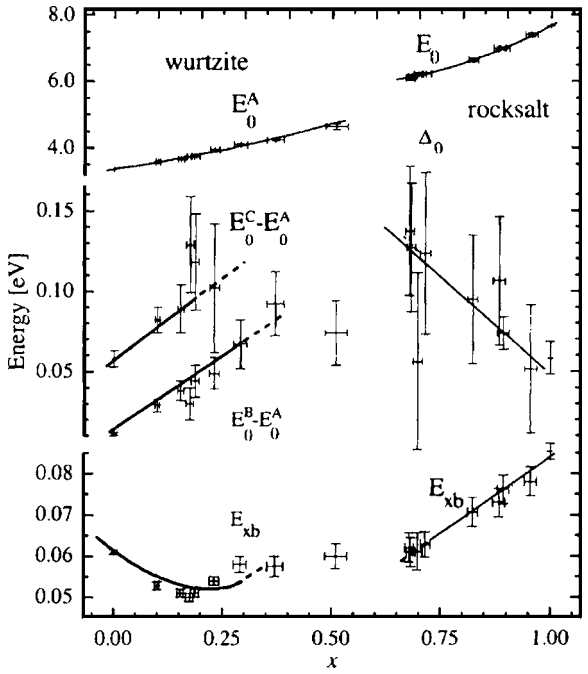

FIG. 7. CP-model parameters for the rocksalt-structure $Mg_xZn_{1-x}O$ band-gap and exciton binding energies E_0, Δ_0, and E_{xb} vs Mg-content x obtained from ellipsometry data analysis using functions for CP-MDF spectra depicted in Fig. 6, and wurtzite-structure $Mg_xZn_{1-x}O$ band-gap and exciton binding energies E_0^A, $E_0^C-E_0^A$, $E_0^B-E_0^A$, and E_{xb} reproduced from Ref. 2. The solid line for the rocksalt-structure composition range connecting data points for E_0 follows Eq. (8). The other lines are drawn as guide to the eye.

sample, the structures merge into broad yet distinct absorption edge, for which all model terms in Eq. (6) are required for successful line shape match. With increasing Zn content, the band-gap energies reveal a distinct redshift, and the absorption edges broaden. The latter is most likely due to the atomic potential fluctuations, common to disordered compounds, and which is leading to locally varying band-gap properties with appearance of absorption tails extending into the band-gap spectral range. For the thin-film samples investigated here, the broadening parameter values of the E_0- and $E_0+\Delta_0$-CP structures are found to be approximately 50 meV, for low Zn contents, with slight increase for alloys with high Zn contents. The free exciton broadening parameters increase from $\Gamma_{xb}\approx 70$ meV($x=1$) to $\Gamma_{xb}\approx 100$ meV($x=0.68$). We attribute the large exciton broadening to dephasing and scattering of the free excitons by local potential fluctuations as well as structural inhomogeneities (defects, grain boundaries) of the $Mg_xZn_{1-x}O$ layers. Therefore, in the experimental $Mg_xZn_{1-x}O$ data, the free exciton CP structures are less pronounced than in the spectra of MgO or ZnO. A similar exciton broadening was observed in the wurtzite-phase $Mg_xZn_{1-x}O$ alloy system.[2]

C. Band-gap and exciton binding energies

1. Band-gap energy

Figure 7 contains the observed dependencies of the CP-MDF model parameters E_0, Δ_0, and E_{xb} on x, together with the wurtzite-structure band-gap and exciton binding energies obtained in our previous work.[2] For $x=1$ the ellipsometric results presented here for the thin films ($E_0=7.674\pm0.005$ eV, $\Delta_{so}=53\pm15$ meV, and $E_{xb}=85.3\pm1.5$ meV) are concordant with data obtained from reflectivity analysis on bulk crystals in Ref. 4 ($E_0=7.77$ eV, $\Delta_{so}=30$ meV, and $E_{xb}=80$ meV) and are highly consistent with those obtained from SE studies on bulk crystals in Ref. 30 ($E_0-E_{xb}=7.6$ eV). With decreasing Mg content, E_0 shifts to lower energies, while the spin-orbit split parameter Δ_0 increases. For the rocksalt-structure alloy system E_0 can be well approximated by a second-order polynomial,

$$E_0(x)[\mathrm{eV}] = 7.6\pm0.5-(7\pm1)x+(7\pm1)x^2, \tag{8}$$

suggesting, although with somewhat large error bars, the band-gap value for virtually unstrained ambient-pressure rocksalt-structure ZnO $E_0(0)=7.6$ eV with strong bowing coefficient of $b=7$ eV. Previous calculations suggest the indirect-gap ($\sim$5.4 eV) high-pressure rocksalt-structure phase of ZnO with a much larger Γ-point band-gap energy [$E_0(0)=6.54$ eV] than its wurtzite-structure counterpart (3.34 eV),[1,32,33] and which is in good agreement with our estimation here.

Between the wurtzite and the rocksalt phases of the alloy system, the band-gap energy parameter E_0 possesses a discontinuity, which amounts to approximately 1 eV.[2] A similar discontinuity was reported from evaluation of absorption edges in transmission measurements in Ref. 16. We attribute this effect to the change of the Zn and Mg coordination in the crystals from fourfold (wurtzite structure) to sixfold (rocksalt structure), which leads to different types of band structures

Downloaded 18 Apr 2007 to 129.93.17.223. Redistribution subject to AIP license or copyright, see http://jap.aip.org/jap/copyright.jsp

and therefore to different values of the band-gap energy with a trend towards higher band-gap energies for the rocksalt structure. A similar trend was also found from local density calculations for rocksalt- versus wurtzite-structure MgO, and for the high-pressure rocksalt-structure ZnO.[32,34]

2. Exciton binding energy

The exciton binding energy parameter E_{xb} decreases approximately linearly with decreasing Mg content, concordant with the reduction of the band gap implying continuous reduction of the conduction and valence band curvatures.[21] Whereas the x dependency of E_{xb} for the wurtzite-structure part reveals a considerable nonlinear behavior,[2] the composition dependence of the binding energy within the rocksalt structure follows a line, which further implies a discontinuity across the phase transition increasing E_{xb} towards the wurtzite-structure part. This behavior can be well understood by the discontinuity of the index of refraction n. The exciton binding energy is proportional to n^{-4}, and hence increases upon the rocksalt-wurtzite phase transition.[21] However, for the latter a precise evaluation of the optical phonon mode discontinuity has to be taken into account and which shall be the subject of further work.

V. CONCLUSIONS

In summary, PLD-grown single-phase, single-crystalline rocksalt-structure $Mg_xZn_{1-x}O$ thin films with $x=0.68-1$ were studied by spectroscopic ellipsometry. We have determined the refractive index dispersion and the model dielectric function parameters for the energy of the fundamental electronic band-to-band transition E_0, the spin-orbit-splitting energy Δ_0, and the exciton binding energy E_{xb} as a function of the Mg-content x upon model line shape analysis of the ellipsometry data. In comparison with the properties of the wurtzite-structure $Mg_xZn_{1-x}O$ it was found that between the two phases E_0 reveals discontinuity due to the bond coordination change in the $Mg_xZn_{1-x}O$ system. The exciton binding energy E_{xb} follows anticipated trends decreasing upon Zn incorporation, and indicates discontinuous behavior across the phase transition. For the rocksalt part, a nearly linear increase of E_{xb} was found between $x=0.68$ and 1 from ≈ 60 to ≈ 85 meV, respectively, which may be promising for use in optoelectronic applications. The large variation of the index of refraction shall permit design of Bragg reflector structures within the rocksalt-structure alloy system.

ACKNOWLEDGMENTS

This work was supported by the Bundesministerium für Bildung und Forschung within the "Wachstumskern INNOCIS" (BMBF Project No. 03WKI09), and the Deutsche Forschungsgemeinschaft GR 1011/10-1 within SPP 1136, and SCHUH 1338/4-1,2 within FOR 404. One of the authors (M.S.) acknowledges startup funds from UNL through EE and CMRA.

[1] G. E. Jellison and L. A. Boatner, Phys. Rev. B **58**, 3586 (1998).
[2] R. Schmidt *et al.*, Appl. Phys. Lett. **82**, 2260 (2003).
[3] Ü. Özgür, Y. I. Alivov, C. Liu, A. Teke, S. D. M. A. Reshchikov, V. Avrutin, S.-J. Cho, and H. Morkoç, J. Appl. Phys. **98**, 041301 (2005).
[4] D. Roessler and W. Walker, Phys. Rev. **159**, 733 (1967).
[5] H. Tanaka, S. Fujita, and S. Fujita, Appl. Phys. Lett. **86**, 192911 (2005).
[6] J. Liang, H. Wu, N. Chen, and T. Xu, Semicond. Sci. Technol. **20**, L15 (2005).
[7] C. Bundesmann, M. Schubert, A. Rahm, D. Spemann, H. Hochmuth, M. Lorenz, and M. Grundmann, Appl. Phys. Lett. **85**, 905 (2004).
[8] A. Ohtomo, M. Kawasaki, T. Koida, K. Masabuchi, H. Koinuma, Y. Sakurai, and Y. Yoshida, Appl. Phys. Lett. **72**, 2466 (1998).
[9] A. Ohtomo, K. Tamura, K. Saikusa, K. Takashi, T. Makino, Y. Segawa, H. Koinuma, and M. Kawasaki, Appl. Phys. Lett. **75**, 2635 (1999).
[10] D. Zhao, Y. Liu, D. Shen, Y. Lu, J. Zhang, and X. Fan, J. Cryst. Growth **234**, 427 (2002).
[11] J. Kang, Y. Park, and K. Kim, Solid State Commun. **115**, 127 (2000).
[12] R. Schmidt-Grund *et al.*, Thin Solid Films **455–456**, 500 (2004).
[13] C. W. Teng, J. F. Muth, Ü. Özgür, M. J. Bergmann, H. O. Everitt, A. K. Sharma, C. Jin, and J. Narayan, Appl. Phys. Lett. **76**, 979 (2000).
[14] A. K. Sharma, J. Narayan, J. F. Muth, C. W. Teng, C. Jin, A. Kvit, R. M. Kolbas, and O. W. Holland, Appl. Phys. Lett. **75**, 3327 (1999).
[15] W. I. Park, G.-C. Yi, and H. M. Jang, Appl. Phys. Lett. **79**, 2022 (2001).
[16] S. Choopun, R. D. Vispute, W. Yang, R. P. Sharma, T. Venkatesan, and H. Shen, Appl. Phys. Lett. **80**, 1529 (2002).
[17] J. Narayan, A. Sharma, A. Kvit, C. Jin, J. Muth, and O. Holland, Solid State Commun. **121**, 9 (2002).
[18] J. Chen, W. Shen, N. Chen, D. Qiu, and H. Wu, J. Phys.: Condens. Matter **15**, L475 (2003).
[19] N. Chen, H. Wu, and T. Xu, J. Appl. Phys. **97**, 023515 (2005).
[20] *Handbook of Ellipsometry*, edited by H. Thompkins and E. A. Irene (William Andrew, Highland Mills,2004).
[21] P. Yu and M. Cardona, *Fundamentals of Semiconductors* (Springer-Verlag, Berlin,1999).
[22] The compensator is an optical element that changes the phase of an incident wave, delaying one of the two orthogonal light constituents. Use of compensators in ellipsometry, in general, allows access to the sign of the ellipsometry parameter Δ, i.e., the handedness of the ellipticity of the plane wave polarization course. Without compensator function, one further loses accuracy in the determination of the ellipsometric parameters when Δ is near 0° or 180°.
[23] M. Schubert, Phys. Rev. B **53**, 4265 (1996).
[24] M. Schubert, *Infrared Ellipsometry on Semiconductor Layer Structures: Phonons, Plasmons and Polaritons* (Springer, New York, 2004).
[25] M. Schubert, in *Introduction to Complex Mediums for Optics and Electromagnetics*, edited by W. S. Weiglhofer and A. Lakhtakia (SPIE, Bellingham, WA, 2004), pp. 677–710.
[26] D. E. Aspnes, in *Handbook of Optical Constants of Solids*, 2nd ed., edited by E. D. Palik (Academic, New York, 1998), Vol. 1.
[27] H. Yao and C. Yan, J. Appl. Phys. **85**, 6717 (1999).
[28] J. Sik, M. Schubert, G. Leibiger, G. Kirpal, V. Gottschalch, and J. Humlíček, Appl. Phys. Lett. **76**, 2859 (2000).
[29] S. Adachi, *GaAs and Related Materials* (World Scientific, New Jersey, 1994).
[30] R. Synowicki and T. E. Tiwald, Thin Solid Films **455–456**, 248 (2004).
[31] *Handbook of Optical Constants of Solids*, edited by E. D. Palik (Academic, New York, 1998), Vol. 3.
[32] J. E. Jaffe, R. Pandey, and A. B. Kunz, Phys. Rev. B **43**, 14030 (1991).
[33] G. E. Jellison, Phys. Rev. B **65**, 049902 (2001).
[34] B. S. Walter, R. L. Lambrecht, S. Limpijumnong, MRS Internet J. Nitride Semicond. Res. **4S1**, G6.8 (1999).
[35] Note that the use of a different model for the surface over layer or the investigation of a smooth $Mg_xZn_{1-x}O$ sample without any additional native surface over layer would result in different absolute values of ε_2, but the general line shape of the dielectric function spectra would not be influenced considerably.

Downloaded 18 Apr 2007 to 129.93.17.223. Redistribution subject to AIP license or copyright, see http://jap.aip.org/jap/copyright.jsp